Journal of Cluster Science, Vol. 13, No. 1, March 2002 (© 2002)

Electronic Structures, (d-p)π Conjugation Effects, and Spectroscopic Properties of Polyoxometalates: $M_6O_{19}^{2-}$ (M = Cr, Mo, W)[1]

Jun Li[2, 3]

Received September 30, 2001

The electronic structures and bonding of isopoly oxometalates $M_6O_{19}^{2-}$ (M = Cr, Mo, W) have been investigated by using *ab initio* and relativistic density functional methods. We have discussed the role of the central oxygen atom and the (d-p)π conjugation interactions between the metal and bridging oxygen atoms. It is found that there exist 12 three-centered two-electron (d-p-d)π bonds for the three $M_4(\mu\text{-O})_4$ planar rings in $M_6O_{19}^{2-}$ ions and these hexametalates are considered to have quasi-aromaticity. The (d-p)π conjugation effects play essential role in stabilizing these cluster compounds, and the reduced (d-p)π conjugation effects account for the instability of the isopoly oxochromate ion, $Cr_6O_{19}^{2-}$. The vibrational spectra and electronic spectra of $M_6O_{19}^{2-}$ ions are evaluated and assigned theoretically and the calculated spectra are in fairly good agreement with the measured experimental results.

KEY WORDS: Polyoxometalate; $M_6O_{19}^{2-}$ isopoly ion; Lindqvist-type metal-oxygen cluster; (d-p)π conjugation effect; three-centered two–electron bond; quasi-aromaticity.

INTRODUCTION

The Lindqvist-type metal-oxygen clusters, $M_6O_{19}^{2-}$ (M = Mo, W), and their functionalized compounds have fascinating chemical properties, photophysical properties, and diverse practical applications [1, 2]. Because of their potential applications in analytical chemistry, electrochemistry,

[1] In memory of Professor Jiaxi Lu.

[2] William R. Wiley Environmental Molecular Science Laboratory, Pacific Northwest National Laboratory, 902 Batelle Boulevard, P.O. Box 999, Richland, Washington 99352. E-mail: jun.li@pnl.gov

[3] Fujian Institute of Research on the Structure of Matter, Chinese Academy of Sciences, Fuzhou, Fujian 35002, China.

1040-7278/02/0300-0137/0 © 2002 Plenum Publishing Corporation

photocatalytic reactions, biological and medical fields, and non-linear optic material sciences, experimental investigations of these isopoly oxometalates have significantly increased in recent years [3, 4]. Even though the M_6O_{19}-type hexachromate counterpart is unknown so far, the hexamolybdate and hexatungstate cluster ions have been synthesized and characterized for a long time [5]. The x-ray structure of $Mo_6O_{19}^{2-}$ cluster was first characterized in 1973 [6], shortly after the reports of its infrared (IR) and Raman spectra [7, 8]. Many compounds with $Mo_6O_{19}^{2-}$ ion are synthesized since then [9]. The single-crystal x-ray structure of $W_6O_{19}^{2-}$ cluster ion was determined in 1978 [10]. In addition, similar hexametalate structures are also known for the group V elements, V [11], Nb [12], and Ta [13]. These isopoly hexametalate ions represent an important group of the metal-oxygen clusters or polyoxometalates.

The fascinating characteristic of these $M_6O_{19}^{2-}$ isopoly anions is that they contain mutually perpendicular $M_4(\mu\text{-}O)_4$ planar rings (Fig. 1), which are also common for many other isopoly or heteropoly anions. The structure of the M-O-M subunits and short M-O distances in these clusters point to the possible existence of (d-p)π conjugation effects in these polyoxometalate systems. It is therefore interesting to explore the role of the (d-p)π conjugation effects and how they affect the electronic structures and properties of these clusters. In addition, the presence of the unique six-coordinate, central oxygen atom in the $M_6O_{19}^{2-}$ clusters requires quantitative theoretical calculations for understanding its effects on the stability of the clusters.

The (d-p)π bonding in transition-metal cluster compounds has been extensively studied by Lu and his colleagues [14]. By comparing with benzene the geometrical structures and chemical reactivities of a series of trinuclear

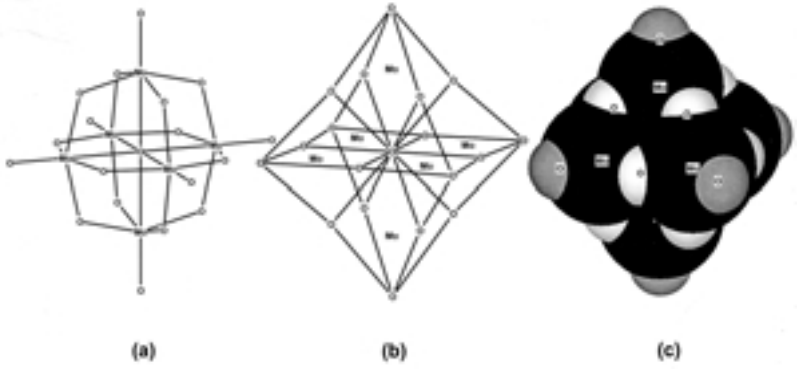

Fig. 1. Molecular structure of the $Mo_6O_{19}^{2-}$ isopoly ion. (a) conventional atom-and-bond representation; (b) octahedron representation; (c) space-filling representation.

incomplete cubane-type M_3X_{13} compounds with $[Mo_3(\mu_3\text{-}S)(\mu\text{-}S)_3]^{4+}$ cluster cores, a new concept, *quasi-aromaticity*, was proposed by Lu and his coworkers to interpret the special stability and reactivities of $[Mo_3S_4]^{4+}$ cluster compounds [15, 16]. The quasi-aromaticity here refers to benzene-like behaviors with regard to chemical reactivities and molecular structures of the cluster compounds. This concept has been found to be helpful in summarizing and interpreting some geometrical features, reactivities, and spectroscopic and magnetic properties of $[M_3S_4]^{4+}$ and $[M_3O_4]^{4+}$ compounds [17, 18]. Semi-empirical (EHMO [19, 20] and CNDO [21]) and *ab initio* [22] theoretical investigations have all shown that there exists a certain degree of (d-p)π conjugation interaction between the d-orbitals of the transition-metal atoms and the p-orbitals of the bridging ligands in the puckered $M_3(\mu\text{-}X)_3$ (X = S, O) six-membered rings. Comparison of the (d-p)π conjugation effects in these $M_4(\mu\text{-}O)_4$ rings to the quasi-aromatic $M_3(\mu\text{-}O)_3$ ring can provide useful information about the nature of the bonding in the $M_6O_{19}^{2-}$ clusters.

Recently, theoretical investigations of several complicated polyoxometalates have become available [23–26]. However, sophisticated theoretical calculations and detailed electronic structure analyses for these highly symmetric $M_6O_{19}^{2-}$ isopoly anions have been surprisingly absent; The only theoretical works on these systems involve two sketchy MO treatments of $Mo_6O_{19}^{2-}$ via the extended Hückel approach [27, 28] and a brief ab initio calculation of the electrostatic potentials of $Mo_6O_{19}^{2-}$ [29], but little information pertaining to bonding and electronic structure is available therefrom. Analyses of the electronic structures of these systems are mainly based on the qualitative MO picture of MO_6 octahedron and empirical *bond length-bond valence relationship* [30]. With the rapid development of computational chemistry, theoretical investigations in terms of state-of-the-art quantum chemical methodologies are now possible for the large-size polyoxometalate systems.

In this paper, we have investigated the electronic structures and bonding of the title compounds by using the relativistic density functional theory (DFT) and *ab initio* methods. Our concerns of these systems are as follows. (1) Can the geometry parameters of these large-size polyoxometalate systems be accurately predicted by using DFT methods? (2) What is the role of the (d-p)π conjugation interactions between the metal and oxygen atoms? (3) What is the bonding nature of the central (μ_6-O) atom in these spherical clusters? (4) Is the $Cr_6O_{19}^{2-}$ cluster thermodynamically stable? (5) Can DFT methods be used to accurately predict the vibrational spectra and electronic spectra of these polyoxometalate clusters? The investigation of these questions will not only shed light on the electronic structure and spectroscopic properties of these isopoly ions, but also

provide helpful guidelines for future theoretical calculations of some more complicated metal-oxygen clusters.

COMPUTATIONAL DETAILS

The theoretical calculations for these polyoxometalates were accomplished by using both DFT methods and ab initio methods. The DFT calculations were performed by using the Amsterdam Density Functional code, ADF 2000 [31]. We used the local density approach (LDA) [32] and generalized-gradient method with Perdew-Wang 91 (PW91) exchange-correlation functionals [33], which had previously been shown to produce accurate geometries and energies for transition-metal systems [34]. Scalar relativistic (mass-velocity and Darwin) effects were taken into account by using the spin-free zero-order regular approximation (ZORA) [35], which was found to work better than the quasi-relativistic method [36] when applied to Cr-, Mo-, W-containing systems [37]. Spin-orbit coupling effects for $W_6O_{19}^{2-}$ were evaluated by using the spin-dependent ZORA formalism with double-group symmetry. Uncontracted triple-zeta Slater-type-orbital (STO) basis sets were used for Cr, Mo, W, and O, with d-type polarization functions for O [38]. Frozen core approximation [31a] was applied to the inner orbitals, i.e., O.1s, Cr.2p, Mo.3d, and W.4f in the ADF notation. All the geometry structures were fully optimized via analytical energy gradient techniques. The frequency calculations were performed at the geometries optimized with scalar relativistic effects included. Two-side displacements were employed in the numerical determination of the force-constant matrices. The vertical excitation energies were calculated at the optimized ground-state geometries by using the time-dependent DFT (TDDFT) method [39], which has been shown to perform very well for transition-metal systems [40–42].

Traditional *ab initio* calculations were also carried out for $Mo_6O_{19}^{2-}$ at the self-consistent-field (SCF) level using the spin-restricted Hartree–Fock scheme [43]. The scalar-relativistic effective core potentials (ECPs) and valence basis set by Hay and Wadt were applied to molybdenum atom [44], while 3–21G all-electron basis set was used for oxygen [45]. To evaluate the degree of electron delocalization, canonical (delocalized) molecular orbitals (CMOs) generated by the SCF procedure were transformed into localized molecular orbitals (LMOs) via Boys localization formalism [46]. Mulliken population analysis [47] was used to evaluate the bond strengths, charge distributions, and percent compositions. All these wavefunction-based calculations were accomplished by using the Gaussian 94 system of programs [48].

RESULTS AND DISCUSSION

Geometries of Isopoly Oxometalates. The $Mo_6O_{19}^{2-}$ geometry structure optimized with the density functional methods is shown in Fig. 1, where the same structure has been shown in three different views: (a) an atom-and-bond representation, (b) a coordination polyhedral representation, and (c) a space-filling representation. The geometries of the Cr and W counterparts are similar. The $M_6O_{19}^{2-}$ (M = Cr, Mo, W) ion has an octahedral M_6 skeleton, with one internal (central) atom, 12 bridging atoms, and six terminal oxygen atoms. For the convenience of discussion, the internal, bridging, and terminal oxygen atoms in $M_6O_{19}^{2-}$ are represented by O_i, O_b, and O_t, respectively. These ions can therefore be written as $M_6(\mu_6\text{-O})(\mu\text{-O})_{12}O_6^{2-}$ or $[Mo(O_i)_{1/6}(O_b)_{4/2}O_t]_6^{2-}$ forms. Here, each M atom is hexa-coordinated by one internal atom, four bridging oxygen atoms, and one terminal atom, forming an MO_6 octahedron with a C_{4v} local symmetry, and the overall symmetry of these isopoly ions are O_h.

These structures can also be viewed as an $M_4(\mu_4\text{-O})(\mu\text{-O})_4O_4$ planar unit being sandwiched by two OMO_4 (C_{4v}) fragments or as six distorted MO_6 octahedrons being connected through common edges with the central atom. The $M_6(\mu\text{-O})_{12}$ cage of these ions are made up of three mutually-perpendicular $M_4(\mu\text{-O})_4$ rings or of 8 puckered $M_3(\mu\text{-O})_3$ six-membered rings fused together.

In Table I we listed the optimized LDA and PW91 bond distances and bond angles, together with the average experimental data. As expected, all the M···M, M-O_i, M-O_b, and M-O_t distances increase from M = Cr to Mo and to W, causing the increase of the cluster size of this $M_6O_{19}^{2-}$ series.

Table I. Optimized and Experimental Geometries of Octahedral $M_6O_{19}^{2-}$ Ions[a]

	M = Cr		M = Mo			M = W		
	LDA	PW91	LDA	PW91	Exp.[b]	LDA	PW91	Exp.[c]
M···M	3.049	3.099	3.283	3.325	3.274	3.312	3.355	3.289
M–O_i	2.156	2.191	2.321	2.351	2.319	2.342	2.372	2.325
M–O_b	1.804	1.836	1.925	1.952	1.928	1.937	1.963	1.924
M–O_t	1.577	1.593	1.712	1.726	1.677	1.735	1.748	1.693
$\angle O_tMO_b$	102.7	102.6	103.5	103.4	103.3	103.8	103.7	103.9
$\angle O_bMO_b$	87.2	87.3	86.9	86.9	86.5	86.8	86.8	87.0
$\angle MO_bM$	115.4	115.1	117.0	116.8	116.4	117.5	117.4	116.9

[a] The theoretical geometries are calculated from LDA and PW91 optimizations.
[b] Reference 6.
[c] Reference 10.

Not surprisingly, the geometry parameters of the Mo and W clusters are close to each other, consistent with the lanthanide contraction and relativistic effects for the third-row transition metals [49, 50].

The optimized LDA bond distances are in good agreement with the experimental values, and they are shorter than the PW91 ones, as usual. For the gradient-corrected PW91 method, although the calculated bond distances are slightly longer than the experimental ones, the agreement between the theoretical and experimental geometries can be improved by including the nearest-neighboring interactions arising from the countercations and the long-range interactions due to the Madelung potentials in the crystal electrostatic fields, as exemplified previously [34, 51].

Electronic Structures and (d-p)π Conjugation Effects

The electronic structures and (d-p)π conjugation effects can be discussed from three aspects: (1) bonding in an MO_6 octahedron, (2) delocalized molecular orbitals, and (3) localized molecular orbitals. In Pope's classification [52], $M_6O_{19}^{2-}$ is a type-I polyanion, i.e., each metal center in the polyanion only has one terminal oxo ligand (mono-oxo). The bonding of the MO_6 octahedron unit, consisting of one terminal triple bonds, four bridging single bonds, and one weak internal single bond, is the basis for qualitative understanding of the electronic structures of these polyanions. We will take $Mo_6O_{19}^{2-}$ as an example in most of the subsequent discussions.

Qualitative Analysis of the Bonding of MoO_6 Octahedron. For the MoO_6 octahedron, it is convenient to assume that the $Mo \equiv O_t$ terminal bonds are along the z-axis, and the four bridging ligands along the x- and y-axis. We have shown in Fig. 2 the correlation of the energy levels of Mo and the MoO_6 unit in O_h and C_{4v} symmetry as well as the (d-p)π conjugation interaction between the lowest unoccupied metallic d-orbital (d_{xy}) and the ligand group orbitals ($a_2 + b_2 + e$ for $4O_b$). Since the hexametalate ions are M(VI) d^0 compounds, all the d-orbitals in MoO_6 are essentially unoccupied. When the octahedron is distorted from O_h to C_{4v} symmetry, the familiar $e_g + t_{2g}$ orbital manifolds in octahedral environment will further be split into MOs with $a_1 + b_1 + b_2 + e$ symmetries [53]. The $Mo \equiv O_t$ triple bonds, made up of a $\sigma(d_{z^2}\text{-}p_z)$ and two $\pi(d_{xz,\,yz}\text{-}p_{x,\,y})$ bonds, and the four Mo-O_b bonds become shorter with the Mo-O_i bond becomes longer. Consequently, the energies of the d_{z^2} and $d_{xz,\,yz}$ orbitals increase, and the $d_{x^2-y^2}$ orbital energy also strongly increases due to the enhancement of the four Mo-O_b bonds.

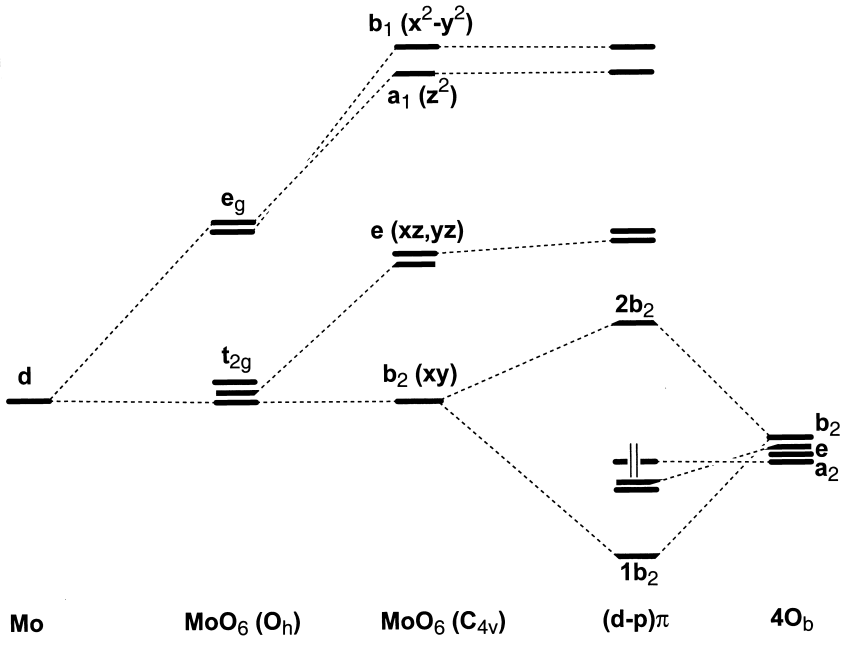

Fig. 2. Energy-level correlation diagram of Mo atom and MoO_6 octahedron with O_h and C_{4v} symmetry. The (d-p)π conjugation interaction is also shown, where the HOMO (a_2) is marked by a two-electron occupation.

If only σ-type orbital interaction is considered, the Mo d_{xy} orbital will be nonbonding because no s-type ligand group orbitals of O_6 have the same symmetry (b_2) in the C_{4v} point group. However, the orientation of this d_{xy} orbital is such that the (d-p)π conjugation interaction between the d_{xy} orbital and π-type ligand group orbitals of the four neighboring O_b can take place. As a result, the $1b_2$ and $2b_2$ MO pair is formed. The $1b_2$ orbital, which is the (d-p)π bonding orbital and mainly O p-orbitals, is stabilized to lie energetically lower than the non-bonding lone pairs in oxygen atoms. Meanwhile, the $2b_2$ orbital, which is the antibonding (d-p)π orbital and mainly Mo d_{xy} orbital, is destabilized and becomes the LUMO. This qualitative bonding picture for MoO_6 was previously discussed via an extended Hückel calculation [27] and has been used to explain the electrochemical properties of $Mo_6O_{19-x}(NR)_x^{2-}$ systems [2c].

Inasmuch as the $Mo_6O_{19}^{2-}$ ion is composed of six MoO_6 octahedrons, the electronic properties can be qualitatively understood from the picture presented above. One can expect that the LUMOs of the $Mo_6O_{19}^{2-}$ ion will mainly be formed from the d_{xy}-type orbitals and the HOMOs should be the

lone-pair orbitals of oxygen atoms. Hence, electrochemical oxidation will involve the ligand lone pairs and reduction will mainly involve the d_{xy}-type metal orbitals. Similarly, the lowest-energy electronic excited-states will be formed via ligand-to-metal charge transfer (LMCT) excitations, as we will discuss below.

Delocalized Molecular Orbitals. In Fig. 3 the MO energy levels of all the $M_6O_{19}^{2-}$ (M = Cr, Mo, W) ions are shown, together with the spin-orbit (SO) energy levels of $W_6O_{19}^{2-}$. With the inclusion of spin-orbit coupling, the triply-degenerate spatial orbitals should split into two components, e.g., $t_{2g} \rightarrow e_{5/2g} + u_{3/2g}$ [54]. However, it is obvious from Fig. 3 that the spin-orbit splittings of the occupied orbitals are negligible because they are

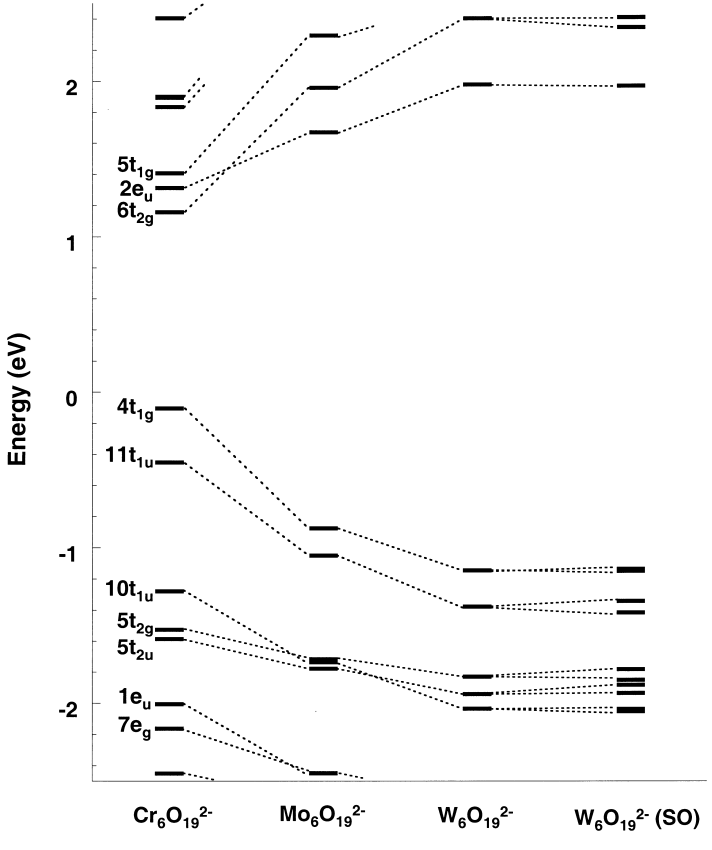

Fig. 3. Energy levels of $M_6O_{19}^{2-}$ (M = Cr, Mo, W). All the energies are calculated by using PW91 method with scalar relativistic effects. The spin-orbit splittings of the levels of $W_6O_{19}^{2-}$ are also shown.

mainly ligand-based orbitals. Even for the metal-based virtual orbitals, the spin-orbit coupling is also small, which is consistent with the well-known fact that the first-order spin-orbit effects vanish for close-shell electronic configurations. Since spin-orbit coupling effects decrease as W ≫ Mo > Cr, we will therefore focus on the electronic structures calculated by only including scalar relativistic effects.

In Fig. 3, the HOMO-LUMO energy gaps of the Mo and W complexes are quite large (2.55 eV and 3.12 eV, respectively), suggesting their stability. Indeed the frequency calculations below indicate that the $Mo_6O_{19}^{2-}$ and $W_6O_{19}^{2-}$ ions are true minima on the potential energy surfaces. On the contrary, as Cr 3d orbitals are quite contracted in the radial distribution by comparing with those of Mo and W, the (d-p)π bonding in the $Cr_6O_{19}^{2-}$ cluster ion is much weaker. Besides, as will be discussed below for the orbital contour plots of $Mo_6O_{19}^{2-}$, the highest occupied $4t_{1g}$ and $11t_{1u}$ MOs are out-of-phase (antibonding) combinations of the lone pairs of the ligands. The smaller cluster size of $Cr_6O_{19}^{2-}$ ion will therefore have higher energy for the HOMOs because of larger ligand-ligand repulsion. These two factors are responsible for a very small HOMO-LUMO energy gap (1.26 eV) for $Cr_6O_{19}^{2-}$. Consequently, the $Cr_6O_{19}^{2-}$ cluster ion is not stable. In fact, frequency calculations (*vide infra*) indicate that the octahedral $Cr_6O_{19}^{2-}$ cluster ion is not a minimum on the potential energy surface, but instead a high-order saddle point with six imaginary frequencies (T_{1u} 111*i* cm^{-1} and T_{1g} 353*i* cm^{-1}). Because of this, the $Cr_6O_{19}^{2-}$ cluster ion will suffer from the second-order Jahn–Teller (SOJT) instability [55]. That is, geometry distortions along the imaginary vibrational modes will lead to more stable structures. This might explain why compounds containing this ion have not been found so far even though similar clusters of the neighboring V and Mo atoms are known.

The eigenvalues and percent compositions for some of the frontier molecular orbitals in $M_6O_{19}^{2-}$ are listed in Table II and the Mulliken net charges, atomic configurations, and atom-atom overlap populations are listed in Table III. From the atomic net charges, the negative charge density increases in the order of $O_t < O_b < O_i$, i.e., the internal O atom possess more electrons than the bridging and terminal O atoms. These results are in contrary to some early bond-valence analysis [8], but they are in agreement with the experimentally observed basicity of these ligands and with the traditional point of view that the $M_6O_{19}^{2-}$ cluster ions can be considered as an O^{2-} ion encapsulated in a M_6O_{18} cage. As expected, the atom-atom overlap populations are consistent with the bonding strength ordering of $M\text{-}O_t \gg M\text{-}O_b \gg M\text{-}O_i$.

Some of the occupied and unoccupied MOs of $Mo_6O_{19}^{2-}$ are illustrated by the stereo contour plots depicted in Figs. 4 and 5, where only

Table II. Orbital Energies (ε_i) and Percent Compositions (%) of Some Frontier MOs of $M_6O_{19}^{2-}$ [a]

	ε_I (eV)	O_i	M	O_b	O_t
		$Cr_6O_{19}^{2-}$			
$2e_u$	1.314	0	46	54	0
$6t_{2g}$	1.159	0	65	32	0
$4t_{1g}$*	−0.103	0	0	99	0
$11t_{1u}$	−0.447	32	0	56	11
$10t_{1u}$	−1.276	14	3	75	7
$5t_{2g}$	−1.524	0	3	41	54
$5t_{2u}$	−1.584	0	3	64	33
$1e_u$	−2.005	0	54	46	0
$7e_g$	−2.160	0	12	87	0
		$Mo_6O_{19}^{2-}$			
$6t_{2g}$	1.959	0	67	32	0
$2e_u$	1.672	0	57	41	0
$4t_{1g}$*	−0.876	0	2	98	0
$11t_{1u}$	−1.050	37	0	48	15
$5t_{2g}$	−1.716	0	1	35	62
$10t_{1u}$	−1.736	12	1	75	10
$5t_{2u}$	−1.777	0	1	57	41
$7e_g$	−2.448	0	6	93	0
$1e_u$	−2.449	0	41	59	0
		$W_6O_{19}^{2-}$			
$6t_{2g}$	2.407	0	70	29	0
$2e_u$	1.982	0	63	36	0
$4t_{1g}$*	−1.139	0	1	99	0
$11t_{1u}$	−1.366	30	0	53	17
$5t_{2g}$	−1.831	0	0	32	65
$5t_{2u}$	−1.941	0	0	52	46
$10t_{1u}$	−2.027	15	2	71	12
$1e_u$	−2.606	0	34	65	0
$9t_{1u}$	−2.690	13	7	18	62

[a] The asterisk denotes the HOMOs.

one-components of the degenerate orbitals are shown for clarity. Obviously, the HOMOs ($4t_{1g}$) of $Mo_6O_{19}^{2-}$ are predominantly formed by the long pairs in the bridging oxygen atoms (cf. Table II), and the SHOMOs ($11t_{1u}$) are formed by the lone pairs of the bridging, terminal, and central ligands. These MOs are out-of-phase combinations of the ligand orbitals, but they are only very weakly antibonding because of the long distances between the ligands. The next block of the occupied MOs, consisting of $5t_{2g}$, $5t_{2u}$,

Table III. Mulliken Net Charges (q), s-, p-, d-type Orbital Populations, and Atom–Atom Overlap Populations (OP_{M-A}) (A = O_i, M, O_b, and O_t) of $M_6O_{19}^{2-}$ (M = Cr, Mo, W)

Atom	q	s	p	d	OP_{M-A}
			M = Cr		
O_i	−1.07	1.88	5.15	0.03	0.14
Cr	1.72	1.96	6.22	4.10	−0.08
O_b	−0.67	1.96	4.68	0.03	0.27
O_t	−0.53	2.00	4.50	0.03	0.32
			M = Mo		
O_i	−1.22	1.91	5.28	0.03	0.09
Mo	2.28	1.86	6.11	3.75	−0.22
O_b	−0.86	1.96	4.88	0.03	0.19
O_t	−0.69	1.98	4.68	0.03	0.34
			M = W		
O_i	−1.20	1.91	5.27	0.03	0.06
W	2.40	2.09	6.13	3.37	−0.10
O_b	−0.90	1.95	4.92	0.03	0.25
O_t	−0.73	1.97	4.73	0.04	0.53

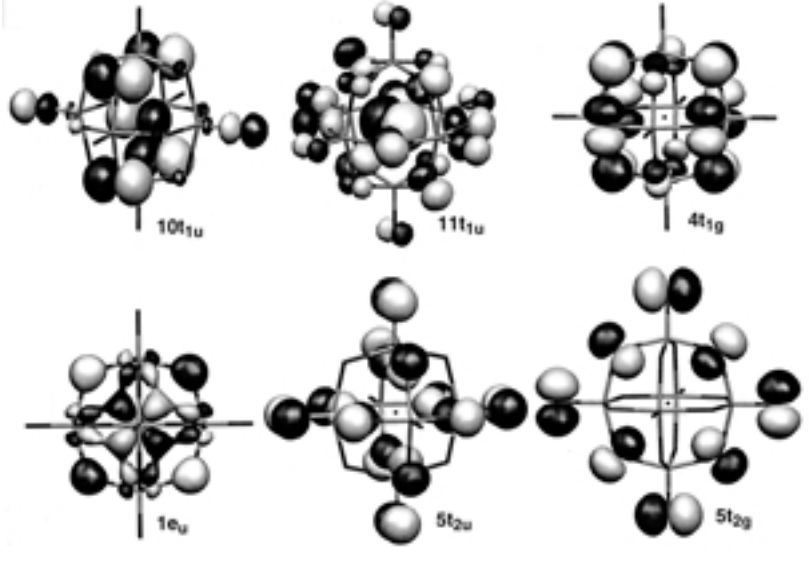

Fig. 4. Contour plots of six frontier occupied molecular orbitals. For the energy-level ordering of these MOs, see Fig. 3.

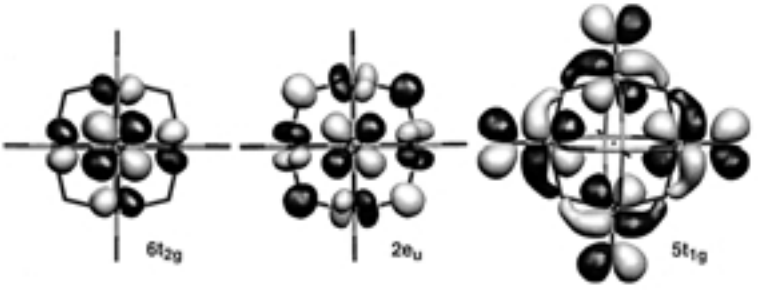

Fig. 5. Contour plots of three lowest-energy unoccupied molecular orbitals. For the energy-level ordering of these MOs, see Fig. 3.

and $10t_{1u}$, are also lone pairs of the ligands and these orbitals are virtually non-bonding.

To analyze the (d-p)π bonding inteactions, it is convenient to use a local coordinate system (LCS) for each M atom, in which all the z-axes points to the center of MO_6 octahedron and all the x-axes lie in the yz-plane of the molecular coordinate system. In such a LCS, the metal skeletal MOs were previously discussed by Hughbanks and Hoffmann [56]. Since the six d_{xy}-type orbitals of the MO_6 units in $M_6O_{19}{}^{2-}$ will transform as $a_{2u}+e_u+t_{2g}$ representations, they will have strong (d-p)π conjugation interaction with the π-type ligand group orbitals that have the same symmetry. Consequently, the ligand-based group orbitals with $a_{2u}+e_u+t_{2g}$ symmetries will be stabilized and the metal-based orbitals with the same symmetries will be destabilized. Indeed, the $1e_u$ orbitals is one of such stabilized MOs that have strong (d-p)π overlap. The LUMOs ($2e_u$ and $6t_{2g}$) are mainly metal-based orbitals with strong mixing of O_b, and they are the antibonding counterparts of the (d-p)π bonding orbitals. Therefore, $Mo_6O_{19}{}^{2-}$ type ions indeed have non-negligible (d-p)π orbital interactions and they will play significant role in the electronic structures and properties of these cluster compounds. The metallic character of the LUMOs is consistent with the fact that these isopoly anions can be electrochemically reduced into $M_6O_{19}{}^{3-}$ ions [57, 58].

The orbitals for the $Mo \equiv O_t$ triple bonds are not shown in Figs. 4 and 5 because they are so strong as to lie energetically far from the frontier MOs. We will not discuss these interactions here. However, the third unoccupied MO ($5t_{1g}$) shown in Fig. 5 is the Mo-O_t antibonding orbital, but this orbital is obviously stabilized due to the in-plane bonding interaction between M and O_b. This latter interaction explains why the antibonding $5t_{1g}$ orbital becomes low-lying.

For the central oxygen atom in $Mo_6O_{19}^{2-}$ cluster, experimental Mo-O_i distances are only 0.14 Å larger than the covalent radii sum of Mo (1.45 Å) and O (0.73 Å) [59]. The O_i atom s- and p(x, y, z)-orbitals, which possess a_{1g} and t_{1u} symmetries under O_h point group, are subject to interacting with the metal group orbitals with the same symmetries [60]. It is therefore certain that there will be indispensable covalent bonding interactions between the skeletal metal atoms and central oxygen atom, even though the interaction is relatively weak due to the long bond distance. The calculated overlap population of Mo-O_t is about as twice bigger as that of Mo-O_b, the overlap population between Mo and the central oxygen atom is as high as 26% and 47% of the overlap populations of Mo-O_t and Mo-O_b. Therefore, the interactions between the central oxygen atom and its six neighboring Mo atoms are not just ionic interactions, but also non-negligible multi-center covalent bonding interactions.

It is interesting to compare the Mo-O_b bond lengths and overlap populations of $Mo_6O_{19}^{2-}$ with those of the quasi-aromatic $[Mo_3(\mu_3\text{-}O)(\mu\text{-}O)_3]^{4+}$ clusters. The Mulliken overlap populations of Mo-(μ-O) and Mo-(μ_3-O) in $[Mo_3O_4]^{4+}$ are 0.278 and 0.461 and the corresponding bond lengths, depending on the peripheral ligands, are 1.90–1.92 Å and 2.01 Å, respectively [22]. From our calculations, the Mo-O_b bond length and overlap populations in $Mo_6O_{19}^{2-}$ are almost the same as in the $[Mo_3O_4]^{4+}$ clusters. The Mo-O_b bond lengths in these clusters lie between those of the Mo-O single bond (2.06 Å) and double bond (1.69 Å) [61], indicating again that (d-p)π conjugation effects play a role in these clusters so that these Mo-O_b bonds have some multiple-bond characters. The similarity of the Mo-O_b bonds in these cluster compounds will be further confirmed by the analysis of the subsequent localized molecular orbitals.

Localized Molecular Orbitals and (d-p)π Conjugation. We will now turn to discuss the localized molecular orbitals of these isopoly ions. LMO technique has been well known to be useful in evaluating degree of delocalization of π-type bonding involving multi-centered interactions and aromatic delocalization [17]. In addition, this approach can provide intuitive chemical pictures that usually agree well with classic valence-bond viewpoints. We have listed the percent compositions, the bonding assignments, and the total number of LMOs in $Mo_6O_{19}^{2-}$ cluster in Table IV, where λ, τ, σ, and π denote the lone pair, banana (bent) bond, σ bond, and π bond, respectively. As usual, banana bonds in LMO calculations come from the mixing of σ- and π-type orbitals.

From Table IV, each terminal O atom in the $Mo_6O_{19}^{2-}$ cluster has one lone pair, and three banana bonds with the Mo atom it attaches to. The formation of the localized triple Mo $\equiv$ O_t bonds is consistent with the short

Table IV. The Percent Compositions, LMO Assignment and the Total Number of the LMOs in $Mo_6O_{19}^{2-}$ [a]

Ligand	Percentage (%)	LMO Assignment	Total
	O(100.0)	λ(O(1s))	19
O_i	Mo(8.3) + O_i(82.6) + Mo(8.3)	σ(Mo–O_i)	4
O_t	Mo(2.7) + O_t(96.6)	λ(Ot)	6
	Mo(31.2) + O_t(69.1)	τ(Mo–O_t)	18
O_b	Mo(3.3) + O_b(91.9) + Mo(3.3)	λ(O_b)	12
	Mo(26.3) + O_b(74.9)	σ(Mo–O_b)	24
	Mo(12.8) + O_b(74.2) + Mo(12.8)	π(Mo–O_b–Mo)	12

[a] λ, τ, σ, and π denote the lone pair, banana bond, σ bond, and π bond, respectively. The LMOs are listed according to the classification of the ligands.

Mo-O_t bond length and with the classical valence bond theory, according to which there should be two covalent bonds and one dative bond from the O_t lone pair to the empty Mo d-orbitals. The existence of the Mo $\equiv$ O_t triple bonds is also in harmony with the long Mo-O_i bonding distance, which is significantly weaker than a normal Mo-O single bond because of the *trans effect* from the triple bonds.

For the internal O atom, there are four LMOs representing the bonding interactions between O_i and Mo atoms. These LMOs are in the large made up of the four s-p hybridized orbitals (lone pairs) of the central oxygen atom, but each LMO possesses significant metal d-orbital characters of at least two of the skeletal Mo atoms. Although the other LMOs are well localized, it is not possible to form a set of four unique LMOs for the bonding between the central atom and the six skeletal Mo atoms. Therefore, the LMO calculations have once again indicated that there are multi-center covalent bonding interactions between O_i and the Mo_6 skeleton.

Based on the preceding delocalized and localized molecular orbital results, the existence of the central oxygen atom in this M_6O_{18} super-octahedron has two effects. On the one hand, the existence of the O_i atom fulfills the octahedral coordination requirement of M atom via electrostatic interaction. On the other hand, the O_i atom can further stabilize the whole ion through its covalent bonding interaction with the skeletal metals. In order to assess the energetic effect of the internal atom on the stability of the $M_6O_{19}^{2-}$ clusters, we have optimized the geometries of the M_6O_{18} super-octahedrons. It turns out that the M_6(M = Cr, M_o, W) skeleton is expanded by 0.103 Å, 0.134 Å, and 0.121 Å, respectively when the O^{2-} ion is removed from the cage. Accordingly, the M $\equiv$ O_t bond distances are

shrunken by 0.031 Å, 0.029 Å, 0.025 Å, respectively. The calculated PW91 "binding energy" for O^{2-} ion and the hollow M_6O_{18} (M = Cr, Mo, W) octahedrons are 17.44 eV, 19.15 eV, and 19.93 eV, respectively. These binding energies are very large, indicating that the internal O_i atom plays a vital part in stabilizing these isopoly ions.

The bonding picture of the bridging O_b atoms in the $Mo_6O_{19}^{2-}$ cluster is even more interesting from the LMO results. According to Table IV, each O_b atom has a lone pair and two σ-type bonds with two neighboring Mo atoms. In addition, the O_b atom is involved in a three-centered two-electron (3c2e) (d-p-d)π bond of the Mo-O_b-Mo unit. This (d-p-d)π bond, arising from the conjugation delocalization of the lone pair electron of O_b into the empty d-orbitals of its two neighboring Mo atoms, is similar with the 3c2e (d-p-d)π bonds that we have discussed in the quasi-aromatic $Mo_3X_4^{4+}$ (X = O, S) cluster compounds [22]. The LMO percent compositions of the 3c2e (d-p-d)π bonds in $Mo_6O_{19}^{2-}$ cluster are close to those calculated for $Mo_3O_4^{4+}$ cluster (Mo(12.0) + O_b(75.7) + Mo(12.0)) [22].

The orbital interactions of the (d-p-d)π bonds on the $Mo_4(\mu\text{-}O)_4$ eight-membered ring of the yz-plane and the side view of these interactions along the x-axis are illustrated in Figs. 6(a) and 6(b). The orbital interactions along the other two $Mo_4(\mu\text{-}O)_4$ rings are the same. Based on analysis of the wavefunctions of the 12 (d-p-d)π LMOs, each Mo atom utilizes its d_{xy}-type orbital (in the LCS) to participate in four inter-adjacent (d-p-d)π bonds. This bonding manner is quite similar to the back-donation interaction between t_{2g} (d_{xy}, d_{xz}, d_{yz}) orbitals and pπ orbitals of four co-planar ligands in ML_6 type octahedral complexes [62], although the orbitals involved here are slightly non-planar. Inasmuch as all the four (d-p-d)π LMOs share exactly the same d_{xy}-type orbital of each Mo atom, the electron cloud of (d-p-d)π LMOs is continuous and closed, and therefore these LMOs can have significant interactions.

As we mentioned previously, $Mo_3X_4^{4+}$ (X = O, S) compounds are transition-metal cluster systems that show quasi-aromaticity. That is, like benzene these clusters show stabilization via electron delocalization by overlapping orbitals of adjacent atoms. Lu and his colleagues have summarized that a quasi-aromatic transition-metal cluster should have strong and extensively delocalized (d-p)π conjugation interactions, and the conjugated orbitals should constitute a continuous, closed (d-p)π system with strong interactions between the localized 3c2e (d-p-d)π bonds [16, 21, 22]. The above LMO analysis indicate that the (d-p-d)π bonds in $Mo_6O_{19}^{2-}$ clusters are also continuous, closed, and have non-negligible interactions with each other. These 3c2e (d-p-d)π bonds at least partially lay the foundation of the stability of this kind of cluster compounds. Therefore the $Mo_6O_{19}^{2-}$ clusters should also be considered as quasi-aromatic, even though

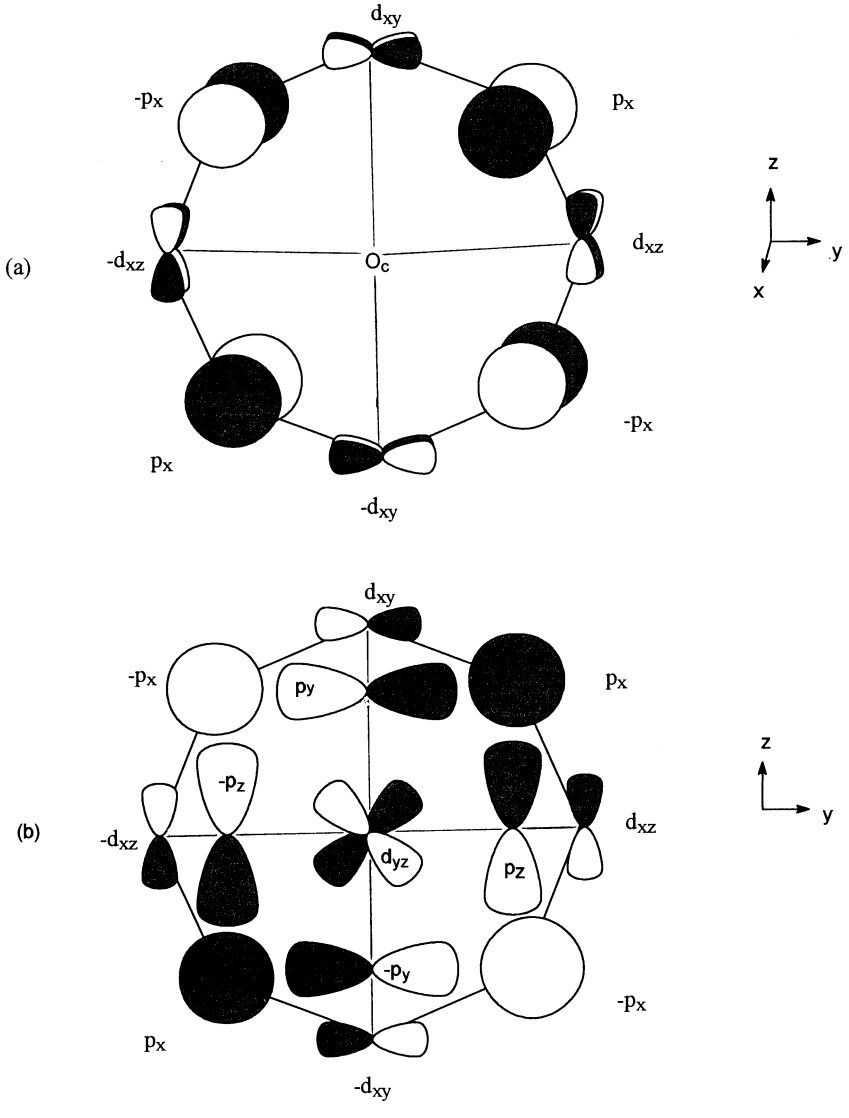

Fig. 6. Orbital interactions of the localized (d-p-d)π bonds in $Mo_6O_{19}^{2-}$: (a) on the $Mo_4(\mu\text{-}O)_4$ ring of the yz-plane; (b) side view along the x-axis. The atomic orbitals are labeled according to the molecular coordinate system shown in the right side.

the (d-p-d)π bonds here are rather weak because of the non-linear structure of the M-O-M units. In fact, the analogy of the interpenetrating $Mo_4(\mu\text{-}O)_4$ rings to the macrocyclic π-bonding systems was noted before [63] and from a topology analysis these $M_6O_{19}^{2-}$ clusters were previously considered to have so-called "binodal aromaticity" by King [64].

Vibrational Properties

The $M_6O_{19}^{2-}$ cluster has 69 vibrational modes, with symmetries $3A_{1g}+1A_{2g}+4E_g+3T_{1g}+4T_{2g}+1A_{1u}+1E_u+7T_{2u}+4T_{1u}$, among which there are only 7 IR-active modes ($7T_{1u}$) and 11 Raman-active modes ($3A_{1g}+4E_g+4T_{2g}$). The calculated LDA and PW91 vibrational frequencies and absorption intensities of the IR modes and frequencies for the Raman-modes of $Mo_6O_{19}^{2-}$ and $W_6O_{19}^{2-}$ ions are listed in Table V. While the calculated PW91 frequencies are slightly worse due to the problem we mentioned in the geometry optimizations, the IR and Raman frequencies

Table V. LDA and PW91 Vibrational Frequencies of the IR and Raman Modes of $M_6O_{19}^{2-}$ (M = Cr, Mo, W)

	$Cr_6O_{19}^{2-}$		$Mo_6O_{19}^{2-}$			$W_6O_{19}^{2-}$		
	LDA	PW91	LDA	PW91	Exp.[a]	LDA	PW91	Exp.[a]
T_{1u}	212	206	198	192	192	167	160	174
	268	251	210	206	220	210	209	226
	394	375	358	349	356	357	348	369
	492	472	447	431	438	430	413	444
	604	573	576	554	602	580	563	586
	768	709	799	776	798	819	778	812
	1034	998	963	934	957	970	942	972
A_{1g}	361	347	289	281	278	230	223	230
	551	525	546	527	580	562	546	557
	1081	1044	994	963	980	993	964	992
E_g	210	198	154	149	197	123	120	178
	460	434	481	461	—	499	481	501
	766	711	807	763	809	840	798	836
	1038	1001	964	935	951	971	942	968
T_{2g}	212	209	194	193	125	172	169	122
	282	274	220	217	163	206	202	215
	475	461	416	412	—	419	416	—
	602	562	586	559	—	568	546	658

[a] The experimental IR and Raman wavenumbers are taken from [8].

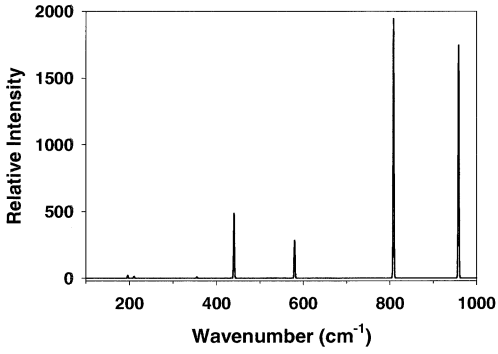

Fig. 7. Theoretical simulated infrared spectrum of $Mo_6O_{19}^{2-}$ ion. The calculated LDA frequencies and intensities are fitted by Gaussina-type functions.

and intensities from LDA calculations agree well with the experiments. In order to illustrate the success of the theoretical calculations of the vibrational spectra of these large metal-oxygen clusters, we have shown in Fig. 7 our simulated IR spectra of $Mo_6O_{19}^{2-}$, where Gaussian-type functions are used to fit the peaks. As shown in Table V and Fig. 7, both the calculated frequencies and the IR intensities are in excellent agreement with experiments. For example, the positions and heights of the peaks in Fig. 7 correspond very well to the experimental frequencies and intensities of $Mo_6O_{19}^{2-}$ at 957 (vs), 798 (vs), 602 (m), 438 (s), 356 (m), 220 (w), and 192 (sh), respectively. Here the intensities are shown as very strong (vs), strong (s), medium (m), weak (w), and shoulder (sh). Similarly, the frequencies and intensities of the four strong IR absorptions for $W_6O_{19}^{2-}$ are calculated at 970 (1348), 819 (2171), 580 (120), and 430 (630) cm^{-1} (km/mol), which again correspond very well with the experimental frequencies and intensities at 972 (vs), 812 (vs), 586 (m), and 444 (s) cm^{-1} (km/mol).

The present DFT calculations of the vibrational frequencies of $Mo_6O_{19}^{2-}$ and $W_6O_{19}^{2-}$ ions have also confirmed previous normal-mode analysis based on various empirical valence force field, where different approximations were applied [65]. The atomic displacements of the six IR-active modes are depicted in Fig. 8, where the lowest-frequency IR mode is not shown because of its very low intensity. Based on the atomic displacements, the three high-frequency IR bands are mainly the stretching modes of M-O_t, M-O_b, and M-O_b-M, while the four low-frequency bands are primarily M-O_b bending and M-O_t bending.

Although the vibrational frequencies of $Mo_6O_{19}^{2-}$ and $W_6O_{19}^{2-}$ ions are all real, one of the T_{1g}-modes of the $Mo_6O_{19}^{2-}$ ion has quite small

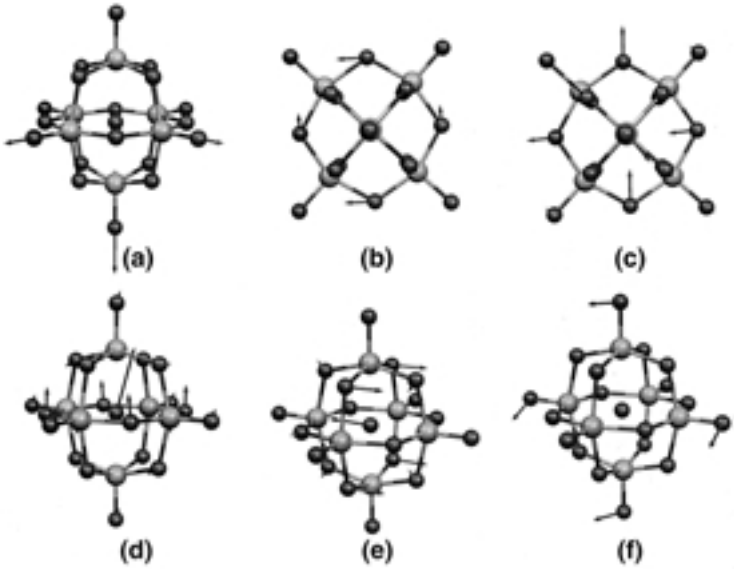

Fig. 8. Atomic displacements of the six IR-active vibrational modes of $Mo_6O_{19}^{2-}$ ion. LDA frequencies: (a) 963 cm^{-1}, (b) 799 cm^{-1}, (c) 576 cm^{-1}, (d) 447 cm^{-1}, (e) 358 cm^{-1}, (f) 210 cm^{-1}.

frequencies (76 cm^{-1}), indicating a very flat potential energy surface regarding to this symmetry coordinate. It was noticed experimentally that the $Mo_6O_{19}^{2-}$ ion experiences "a slight distortion of the octahedron that involves the bridging bonds on the surface of the cage" [6]. The structural irregularity is generally less significant for $W_6O_{19}^{2-}$ than for $Mo_6O_{19}^{2-}$. Our calculated low-frequency vibrational modes of $Mo_6O_{19}^{2-}$ are depicted in Fig. 9. It is clear that vibrations along this low-frequency mode will give rise to a short-and-long alternative Mo=O···Mo arrangement in the two

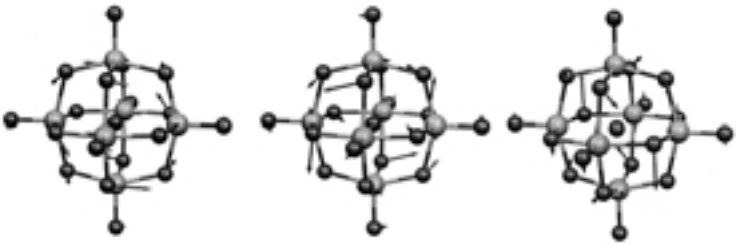

Fig. 9. Atomic displacements of the three components of the low-frequency T_{1g}-mode of the $Mo_6O_{19}^{2-}$ ion.

$OMoO_4$ fragments and a slightly puckered $M_4(\mu_4\text{-}O)(\mu\text{-}O)_4O_4$ ring. Therefore, a slightly distorted octahedral structure of $Mo_6O_{19}^{2-}$ should be energetically close to the regular structure with O_h symmetry. This result is consistent with the experimental finding mentioned above and with the theoretical argument for an asymmetric linear M-X-M linkage [66]

As mentioned previously, the $Cr_6O_{19}^{2-}$ ion has two sets of large imaginary frequencies at $358i$ cm^{-1} for T_{1g} and $120i$ cm^{-1} for T_{1u}. The vibrational frequencies of this ion are therefore not listed in Table V. To verify whether the imaginary frequencies of the $Cr_6O_{19}^{2-}$ ion are due to numerical noises for low-frequency modes, we used very tight criteria for the self-consistent-field convergence and geometry optimizations and increased the integration accuracy from the default INTEGRATION = 6.0 to 8.0 and to 10.0. It turns out that the imaginary frequencies remain unchanged for the $Cr_6O_{19}^{2-}$ ion. Therefore this ion will indeed subject to second-order Jahn-Teller instabilities [55], as we discussed before.

Electronic Spectra

The characteristics of the electronic spectra of polyoxometalates are useful in understanding their electronic structures [67]. Although it is generally agreed that the first electronic transition band involves ligand-metal charge transfer, first-principle theoretical analysis is still lack. The success of time-dependent DFT methods in predicting and assigning electronic spectra of transition-metal systems has been exemplified recently [40, 41]. We will therefore employ this new methodology to explore the electronic transitions of the polyoxometalates. Before we perform TDDFT calculations on these large isopoly ions, we take MoO_4^{2-} ion as a benchmark to verify the reliability of the TDDFT calculation of electronic spectra of the polyoxometalates. The electronic absorptions of the MoO_4^{2-} ion in the Na_2MoO_4 crystal are 260 and 225 nm, corresponding to excitation energies of 4.77 and 5.51 eV, respectively [68]. For the transitions from the ground state ($^1A_1$) to the first and second $^1T_2$ excited states of MoO_4^{2-} ion, our calculated excitation energies on the optimized geometries are 4.02 and 5.02 eV (LDA) and 3.67 and 4.84 eV (PW91), respectively. Since the effects of the counter-cations and the Madelung potentials have not been taken into account in our calculations, the optimized bond distances of the free MoO_4^{2-} ion are too long and the excitation energies are underestimated as a result. Even so, the calculated LDA excitation energies are still fairly useful in discussing the electronic transitions in these systems. Therefore, we will only use the LDA excitation energies for the large systems.

The calculated excitation energies, absorption wavelengths, and the oscillator strengths for the electric-dipole-allowed (T_{1u} symmetry) electronic excitations of the $Mo_6O_{19}^{2-}$ and $W_6O_{19}^{2-}$ ions are listed in Table VI. The experimentally measured absorption wavelengths and the molar extinction coefficients for the electronic spectra are also listed for comparison [69, 70]. Experimentally, $Mo_6O_{19}^{2-}$ ion has two electronic absorptions at 3.82 and 4.82 eV, respectively. Our LDA calculations indicate that the first two electronic excitations of this ion lie at 3.03 eV ($4t_{1g} \rightarrow 2e_u$, HOMO $\rightarrow$ LUMO) and 3.24 eV ($11t_{1u} \rightarrow 6t_{2g}$, HOMO-1 $\rightarrow$ LUMO+1). These two excitations are both of LMCT type and should be responsible for the experimental peak observed at 325 nm. The third excitation is calculated at 3.57 eV ($11t_{1u} \rightarrow 5t_{1g}$, HOMO-1 $\rightarrow$ LUMO+2), which should correspond to the experimental peak at 260 nm. For the $W_6O_{19}^{2-}$ ion, there are two experimental peaks at 4.43 and 5.93 eV. The calculated LDA excitation energies are at 3.59 eV ($4t_{1g} \rightarrow 2e_u$) and 3.99 eV ($11t_{1u} \rightarrow 6t_{2g}$). The assignments for the electronic transitions listed in the parenthesis are for the main configurations.

Table VI. LDA and PW91 Excitation Energies (ΔE), Absorption Wavelengths (λ), and Oscillator Strengths (f) for the Electric–Dipole Allowed Electronic Transitions

	PW91			LDA			Exp.[a]		
	ΔE (eV)	λ (nm)	$10^3 f$	ΔE (eV)	λ (nm)	$10^3 f$	ΔE (eV)	λ (nm)	$10^{-3}\varepsilon$
				$Mo_6O_{19}^{2-}$					
aT_{1u}	2.856	435	23.2	3.027	410	25.5	3.815	325	9.0
bT_{1u}	3.075	404	25.7	3.245	383	27.7			
cT_{1u}	3.382	367	19.5	3.551	350	0.2			
dT_{1u}	3.427	362	2.8	3.566	348	25.8	4.824	260	17.6
eT_{1u}	3.764	330	0.1	3.904	318	0.1			
fT_{1u}	3.822	325	2.6e–3	4.038	307	1.8e–2			
gT_{1u}	3.847	323	0.2	4.058	306	0.4			
				$W_6O_{19}^{2-}$					
aT_{1u}	3.442	361	52.1	3.593	346	54.6	4.428	280	11.0
bT_{1u}	3.820	325	9.2	3.926	316	0.7			
cT_{1u}	3.866	321	25.1	3.992	311	33.9	5.932	209	19.5
dT_{1u}	4.217	294	24.7	4.360	285	28.0			
eT_{1u}	4.374	284	0.3	4.486	277	0.2			
fT_{1u}	4.604	270	0.1	4.790	259	0.3			
gT_{1u}	4.627	268	6.6	4.811	258	12.8			

[a] The experimental electronic absorption wavelengths are taken from [69] and [70] and the experimental molar extinction coefficients (ε) are in $mol^{-1} \cdot L \cdot cm^{-1}$.

These calculated excitation energies for the free hexametalate ions are systematically lower than the excitation energies derived from the experimental maximum absorption wavelengths measured in solutions [69, 70]. We have also performed calculations that include solvent effects via a dielectric continuum self-consistent-reaction-field model and there is no significant improvement. Obviously, the metal-ligand interactions are underestimated in our calculations for the free ions. More accurate calculations of these excitation energies will need to include the counter-cations and to use a super-cluster model for the solvation shells. We will not pursue such calculations in the present work.

CONCLUSIONS

We have performed relativistic DFT and ab initio calculations on the Lindqvist-type $M_6O_{19}^{2-}$ isopoly oxometalate ions. The calculated structural parameters via DFT geometry optimizations are close to the experimental measurements. Qualitative analysis of the bonding of the MO_6 octahedron reveals the possibility of significant (d-p)p conjugation interactions within the spherical M_6O_{12} cage, which has been confirmed by the calculated delocalized and localized molecular orbitals. It is shown that there are crucial (d-p)π conjugation interactions between the empty d orbitals of M atoms and the occupied p orbitals (lone pair) of the bridging atoms. When the (d-p)π bonding orbitals are transformed via localized molecular orbital technique, 12 three-centered two-electron (d-p-d)π bonds are formed within the three $M_4(\mu\text{-}O)_4$ planar rings of the $M_6O_{19}^{2-}$ ions. Inasmuch as these localized (d-p-d)π bonds are continuous, closed, and have non-negligible interaction with each other, these isopoly oxometalate ions are considered to be quasi-aromatic, i.e., they are stabilized via electron delocalization by overlapping orbitals of adjacent atoms. The (d-p)π conjugation effects or the quasi-aromaticity are partially responsible for the stability of these polyoxometalate clusters.

Contrary to the stability of the Mo and W counterparts, the $Cr_6O_{19}^{2-}$ ion is not stable in an octahedral structure. Because of the large ligand repulsion and small (d-p)π interaction, this ion only has a very small HOMO-LUMO energy gap. The frequency calculations indicate that the octahedral hexachromate ion is only a high-order saddle point on the potential energy surface and it will be subject to the second-order Jahn-Teller instability, which explains the mysterious absence of this ion so far.

We have also discussed the effect of the central μ_6-O atom. It is found that there are significant multi-center covalent bonding interactions between the central oxygen atom and skeletal M atoms in the $M_6O_{19}^{2-}$ cluster. Encapsulation of the O^{2-} ion in the $M_6O_{19}^{2-}$ cage has unexpectedly

large energetic effects. It is therefore clear that the central atom in these clusters is not just a trivial ligand fulfilling electrostatic coordination requirement, but also an indispensable atom that provides covalent bonding to the M_6 skeleton. The central atom is hence an important factor for stabilization of these unique spherical clusters.

The calculated infrared and Raman vibrational frequencies and theoretical infrared absorption intensities are in good agreement with experiments, indicating the power of the DFT methods in predicting, explaining, and assigning vibrational modes of these complicated cluster ions. The first-principle accurate calculations of the vibrational properties have provided another avenue for understanding vibrational properties, in addition to the traditional normal-mode analysis via empirical valence force-field approaches, where various approximations have to be adopted. The accurate predictions of the vibrational properties of these polyoxometalate clusters pave the way for further investigation of other properties, e.g., non-linear optic properties, of some isopoly or heteropoly metal-oxygen clusters.

In order to understand the electronic spectra of these isopoly ions, we have also explored the electronic transitions via time-dependent DFT theory. It is found that the two peaks of $Mo_6O_{19}^{2-}$ and $W_6O_{19}^{2-}$ in the visible regions mainly correspond to the HOMO $\rightarrow$ LUMO and HOMO-1 $\rightarrow$ LUMO + 1 transitions. Both these transitions belong to the ligand-metal charge-transfer (LMCT) type, consistent with their large experimental molar extinction coefficients. Although the calculations provided useful information about the nature of the electronic transitions involved in the electronic spectra, the calculated electronic excitation energies for the free ions are not in quantitative agreement with the experimental electronic spectra of these ions. Further calculations that include the solvation or crystal environments and count-cations are needed if quantitative agreement is sought.

ACKNOWLEDGMENTS

The Computational Center of Fujian Province (China) and the Ohio Supercomputer Center are acknowledged for computer time. The National Natural Sciences Foundation of China and the Foundation of State Key Laboratory of Structural Chemistry are acknowledged for grants in support of this work.

REFERENCES

1. (a) M. T. Pope, *Heteropoly and Isopoly Oxometalates* (Springer-Verlag, New York, 1983).
(b) M. T. Pope, *in* S. J. Lippard (ed.), *Progress in Inorganic Chemistry* (Wiley, New York,

1991), Vol. 39, p. 181. (c) M. T. Pope and A. Müller (eds.), *Polyoxometalates: from Platonic Solids to Retro-viral Activity* (Kluwer Academic Publishers, Dodrecht, The Netherlands, 1994). (d) C. L. Hill (ed.) (1996). A special issue on polyoxometalates in catalysis, *J. Mol. Catalysis A: Chem.* **114**, 1–371. (e) C. L. Hill (ed.) (1998). A special issue on polyoxometalates, *Chem. Rev.* **98**, 1–390.

2. (a) P. Gouzerh, Y. Jeannin, A. Proust, F. Robert, and S.-G. Roh (1993). *Mol. Eng.* **3**, 79. (b) P. Gouzerh and A. Proust (1998). *Chem. Rev.* **98**, 77. (c) J. B. Strong, G. P. A. Yap, R. Ostrander, L. M. Liable-Sands, A. L. Rheingold, R. Thouvenot, P. Gouzerh, and E. A. Maatta (2000). *J. Am. Chem. Chem.* **122**, 639. (d) W. Clegg, R. J. Errington, K. A. Fraser, C. Lax, and D. G. Richards, *in* M. T. Pope and A. Müller (eds.), *Polyoxometalates: from Platonic Solids to Retro-Viral Activity* (Kluwer Academic Publishers, Dordrecht, The Netherlands, 1994).
3. (a) M. T. Pope and A. Müller (1991). *Angew. Chem., Intl. Ed. Engl.* **30**, 34. (b) V. W. Day and W. G. Klemperer (1985). Science **288**, 533. (c) Y. Hou and C. L. Hill (1993). *J. Am. Chem. Soc.* **115**, 11823. (d) Y. Lin, T. J. R. Weakley, B. Rapko, and R. G. Finke (1993). *Inorg. Chem.* **32**, 5095.
4. (a) M. T. Pope, *in* D. B. Brown (ed.), *Mixed-Valence Compounds* (D. Reidel Publishing, Dordrecht, The Netherlands, 1980), p. 365. (b) B. Krebs, *in* A. Müller and E. Diemann (eds.), *Transition Metal Chemistry* (Verlag Chemie, Weinheim, Germany, 1981), p. 91. (c) R. I. Buckley and R. J. H. Clark (1985). *Coord. Chem. Rev.* **65**, 167. (d) C. J. Young (1989). *Coord. Chem. Rev.* **96**, 89. (e) D. E. Katsoulis (1998). *Chem. Rev.* **98**, 359.
5. H. T. Evans, Jr. (1971). *Perspect. Struct. Chem.* **4**, 1.
6. (a) H. R. Allcock, E. C. Bissell, and E. T. Shawl (1973). *Inorg. Chem.* **12**, 2963. (b) H. R. Allcock, E. C. Bissell, and E. T. Shawl (1972). *J. Am. Chem. Chem.* **94**, 8603.
7. J. Fuchs and K. Jahr (1968). *Z. Naturforsch. B* **23**, 1380.
8. R. Mattes, H. Bierbusse, and J. Fuchs (1971). *Z. Anorg Allg. Chem.* **385**, 230.
9. (a) C. D. Garner, N. C. Howlander, F. E. Mabbs, A. T. McPhail, R. W. Miller, and K. D. Onan (1978). *J. Chem. Soc., Dalton Trans.* 1582. (b) O. Nagano and Y. Sasaki (1979). *Acta Crystallogr.* **B35**, 2387. (c) W. Clegg, G. M. Sheldrick, C. D. Garner, and I. B. Walton (1982). *Acta Crystallogr.* **B38**, 2906. (d) P. Dahlstrom, J. Zubieta, B. Neaves, and J. R. Dilworth (1982). *Cryst. Struct. Commun.* **11**, 463. (e) H. Arzoumanian, A. Baldy, R. Lai, A. Odreman, J. Metzger, and M. Pierrot (1985). *J. Organomet. Chem.* **295**, 343. (f) C. B. Shoemaker, L. V. McAfee, D. P. Shoemaker, and C. W. DeKock (1986). *Acta Crystallogr.* **C42**, 1310. (g) V. Riera, M. A. Ruiz, F. Villafane, Y. Jeannin, and C. Bois (1988). *J. Organomet. Chem.* **345**, C4. (h) S. F Lu, J. Q. Huang, Z. X. Huang, and J. L. Huang (1989). *J. Struct. Chem.* **8**, 27. (i) C. Zhang, Y. Ozawa, Y. Hayashi, and K. Isobe (1989). *J. Organomet. Chem.* **373**, C21. (j) S. N. Bernstein and K. R. Dunbar (1992). *Angew. Chem., Int. Ed. Engl.* **31**, 1360. (k) X.-X. Xu, X.-Z. You, and X.-Y. Huang (1995). *Polyhedron* **14**, 13. (l) D. Wu, S. Wang, X. Lin, C. Lu, and H. Zhuang (2000). *Acta Cryst. C* **56**, e55.
10. (a) J. Fuchs, W. Freiwald, and H. Hartl (1978). *Acat Cryst.* **B34**, 1764. (b) J. Fuchs (1973). *Z. Naturforsch.* **B28**, 389.
11. (a) Y. Hayashi, Y. Ozawa, and K. Isobe (1989). *Chem. Lett.* 425. (b) H. K. Chae, W. Klemperer, and V. W. Day (1989). *Inorg. Chem.* **28**, 1423. (c) Y. Hayashi, Y. Ozawa, and K. Isobe (1991). *Inorg. Chem.* **30**, 1025.
12. (a) I. Lindqvist (1952). *Ark. Kemi* **5**, 247. (b) A. Goiffon, E. Philippot, and M. Maurin (1980). *Rev. Chim. Miner.* **17**, 466.
13. I. Lindqvist and B. Aronsson (1954). *Ark. Kemi* **7**, 49.
14. J. X. Lu, *New Developments in Transition Metal Cluster Chemistry* (Science Press New York, New York, 2000).

15. (a) J. Q. Huang, J. L Huang, M. Y. Shang, S. F. Lu, X. T. Lin, Y. H. Lin, M. D. Huang, H. H. Zhuang, and J. X. Lu (1988). *Pure Appl. Chem.* **60**, 1185. (b) J. Q. Huang, S. F. Lu, M. Y. Shang, X. T. Lin, M. D. Huang, Y. H. Lin, D. M. Wu, H. H. Zhuang, J. L Huang, and J. X. Lu (1987). *J. Struct. Chem.* **6**, 219. (In Chinese)
16. J. X. Lu (1989). *J. Struct. Chem.* **8**, 327. (In Chinese)
17. J. X. Lu and Z. D. Chen (1994). *Int. Rev. Phys. Chem.* **13**, 85 (Taylor & Francis, London).
18. J. Li, Ph.D. Dissertation (Fujian Institute of Research on the Structure of Matter, Chinese Academy of Sciences, 1991).
19. (a) J. Q. Li and W. D. Cheng (1987). *J. Mol. Struct. (Theochem)* **151**, 19. (b) J. Q. Li (1988). *J. Mol. Struct. (Theochem)* **181**, 185.
20. (a) W. D. Cheng, Q. E. Zhang, J. S. Huang, and J. X. Lu (1989). *Polyhedron* **8**, 2785. (b) W. D. Cheng, Q. E. Zhang, J. S. Huang, and J. X. Lu (1990). *Polyhedron* **9**, 1625.
21. (a) Z. D. Chen, J. Li, W. D. Chen, J. Q. Huang, C. W. Liu, Q. E. Zhang, and J. X. Lu (1990). *Chin. Sci. Bull.* **35**, 1698. (b) Z. D. Chen, J. X. Lu, C. W. Liu, and Q. E. Zhang (1991). *Polyhedron* **10**, 2799.
22. (a) J. Li, C. W. Liu, and J. X. Lu, *Book of Abstracts: The 7th International Congress of Quantum Chemistry* (Menton, France, 1991), p. 249. (b) J. Li, C. W. Liu, and J. X. Lu (1994). *J. Chem. Soc., Faraday Trans.* **90**, 39. (c) J. Li, C. W. Liu, and J. X. Lu (1994). *Polyhedron* **13**, 1841. (d) J. Li, C. W. Liu, and J. X. Lu (1996). *J. Cluster Chem.* **7**, 469.
23. R.-M. Rohmer, M. Bénard, J.-P. Blaudeau, J.-M. Maestre, and J.-P. Poblet (1998). *Coord. Chem. Rev.* **178–180**, 1019.
24. J. M. Maestre, J. P. Sarasa, C. Bo, and J. M. Poblet (1998). *Inorg. Chem.* **37**, 3071.
25. (a) X. López, J. M. Maestre, C. Bo, and J.-M. Poblet (2001). *J. Am. Chem. Soc.* **123**, 9571. (b) J. M. Maestre, X. López, C. Bo, J.-M. Poblet, and N. Casañ-Pastor (2001). *J. Am. Chem. Soc.* **123**, 3749. (c) J. M. Maestre, J.-M. Poblet, C. Bo, N. Casañ-Pastor, and P. Gomez-Romero (1998). *Inorg. Chem.* **37**, 3444.
26. H. Duclusaud and S. A. Borshch (2001). *J. Am. Chem. Soc.* **123**, 2825.
27. D. Masure, P. Chaquin, C. Louis, M. Che, and M. Fournier (1989). *J. Catalysis* **119**, 415.
28. M. J. Calhorda (1994). *J. Organomet. Chem.* **475**, 149.
29. A. Dolbecq, A. Guirauden, M. Fourmigué, K. Boubekeur, P. Batail, M.-M. Rohmer, M. Bénard, C. Coulon, M. Sallé, and P. Blanchard (1999). *J. Chem. Soc., Dalton Trans.* 1241.
30. D. M. P. Mingos (Ed.) (1999). *Struct. & Bonding* **93**, 1–321.
31. *ADF 2000.02* (Theoretical Chemistry, Vrije Universiteit, Amsterdam), (http://www.scm.com). (a) E. J. Baerends, D. E. Ellis, and P. Ros (1973). *Chem. Phys.* **2**, 41. (b) L. Versluis and T. Ziegler (1988). *J. Chem. Phys.* **88**, 322. (c) G. te Velde and E. J. Baerends (1992). *J. Comput. Phys.* **99**, 84. (d) C. Fonseca Guerra, J. G. Snijders, G. te Velde, and E. J. Baerends (1998). *Theor. Chem. Acc.* **99**, 391.
32. (a) J. C. Slater, *Quantum Theory of Molecular and Solids, Vol. 4* (McGraw-Hill, New York, 1974). (b) S. H. Vosko, L. Wilk, and M. Nusair (1980). *Can. J. Phys.* **58**, 1200.
33. J. P. Perdew and Y. Wang (1992). *Phys. Rev. B* **45**, 13244. (b) J. P. Perdew, J. A. Chevary, S. H. Vosko, K. A. Jackson, M. R. Pederson, D. J. Singh, and C. Foilhais (1992). *Phys. Rev. B* **46**, 6671.
34. J. Li and K.-C. Wu (2000). *Inorg. Chem.* **39**, 1538.
35. E. van Lenthe, E. J. Baerends, and J. G. Snijders (1993). *J. Chem. Phys.* **99**, 4597.
36. T. Ziegler, E. J. Baerends, J. G. Snijders, and W. Ravenek (1989). *J. Phys. Chem.* **93**, 3050.
37. B. E. Bursten, M. H. Chisholm, C. M. Hadad, J. Li, and P. J. Wilson (2001). *Chem. Commun.* In press.

38. (a) J. G. Snijder, E. J. Baerends, and P. Vernooijs (1982). *At. Nucl. Data Tables* **26**, 483. (b) P. Vernooijs, J. G. Snijder, and E. J. Baerends, *Slater Type Basis Functions for the Whole Periodic System*, Internal Report, (Free University of Amsterdam, The Netherlands, 1984).
39. S. J. A. van Gisbergen, J. G. Snijders, and E. J. Baerends (1999). *Comp. Phys. Comm.* **118**, 119.
40. A. Rosa, E. J. Baerends, S. J. A. van Gisbergen, E. van Lenthe, J. A. Groeneveld, and J. G. Snijders (1999). *J. Am. Chem. Soc.* **121**, 10356.
41. K. Wakamatsu, K. Nishimoto, and T. Shibahara (2000). *Inorg. Chem. Commun.* **3**, 677.
42. E. Broclawik and T. Borowski (2001). *Chem. Phys. Lett.* **339**, 433.
43. C. C. J. Roothaan (1951). *Rev. Mod. Phys.* **23**, 69.
44. (a) P. J. Hay and W. R. Wadt (1985). *J. Chem. Phys.* **82**, 270.
45. W. J. Hehre, R. F. Stewart, and J. A. Pople (1969). *J. Chem. Phys.* **51**, 2657.
46. (a) S. F. Boys (1960). *Rev. Mod. Phys.* **32**, 296. (b) J. M. Foster and S. F. Boys (1960). *Rev. Mod. Phys.* **32**, 300.
47. R. S. Mulliken (1955). *J. Chem. Phys.* **23**, 1833.
48. M. J. Frisch, G. W. Trucks, H. B. Schlegel, P. M. W. Gill, B. G. Johnson, M. A. Robb, J. R. Cheeseman, T. A. Keith, G. A. Petersson, J. A. Montgomery, K. Raghavachari, M. A. Al-Laham, V. G. Zakrzewski, J. V. Ortiz, J. B. Foresman, J. Cioslowski, B. B. Stefanov, A. Nanayakkara, M. Challacombe, C. Y. Peng, P. Y. Ayala, W. Chen, M. W. Wong, J. L. Andres, E. S. Replogle, R. Gomperts, R. L. Martin, D. J. Fox, J. S. Binkley, D. J. Defrees, J. Baker, J. P. Stewart, M. Head-Gordon, C. Gonzales, and J. A. Pople, *Gaussian 94* (Gaussian, Pittsburgh, PA).
49. P. Pyykkö (1979). *Phys. Scr.* **20**, 647.
50. (a) M. Seth, M. Dolg, P. Fulde, and P. Schwerdtfeger (1995). *J. Am. Chem. Soc.* **117**, 6597. (b) W. Küchle, M. Dolg, and H. Stoll (1997). *J. Phys. Chem. A* **101**, 7128.
51. J. Li, S. Irle, and W. H. E. Schwarz (1996). *Inorg. Chem.* **35**, 100.
52. M. T. Pope (1972). *Inorg. Chem.* **11**, 1973.
53. T. A. Albright, J. K. Burdett, and M.-H. Whangbo, Orbital Interactions in Chemistry (John-Wiley & Sons, New York, 1985), p. 314.
54. J. A. Salthouse and M. J. Ware, *Point Group Character Tables and Related Data* (Cambridge University Press, London, 1972).
55. J. Li, C.-W. Liu, and J.-X. Lu (1993). *J. Mol. Struct. (Theochem)* **280**, 223.
56. T. Hughbanks and R. Hoffmann (1983). *J. Am. Chem. Soc.* **105**, 1154.
57. C. Sanchez, J. Livage, J. P. Launay, M. Fournier, and Y. Heannin (1982). *J. Am. Chem. Soc.* **104**, 3194.
58. P. L. Veya and J. K. Kochi (1995). *J. Organomet. Chem.* **488**, C4.
59. W. W. Porterfield, *Inorganic Chemistry, A Unified Approach*, 2nd ed. (Academic Press, San Diego, 1993).
60. T. A. Albright, J. K. Burdett, and M.-H. Whangbo, *Orbital Interactions in Chemistry* (Wiley, New York, 1985), p. 438 .
61. A. G. Orpen, L. Brammer, F. H. Allen, O. Kennard, D. G. Watson, and R. Taylor (1989). *J. Chem. Soc., Dalton Trans.* Supplement, S68.
62. F. A. Cotton, *Chemical Applications of Group Theory*, 3rd ed. (Wiley, New York, 1990), p. 231.
63. K. Nomiya and M. Miwa (1984). *Polyhedron* **3**, 341.
64. R. B. King (1991). *Inorg. Chem.* **30**, 4437.
65. (a) F. J. Farrell, V. A. Maroni, and T. G. Spiro (1969). *Inorg. Chem.* **8**, 2638. (b) R. Mattes, H. Bierbuesse, and J. Fuchs (1971). *Z. Anorg. Allg. Chem.* **385**, 230. (b) C. Rocchiccioli-Deltcheff, R. Thouvenot, and M. Fouassier (1982). *Inorg. Chem.* **21**, 30.

(c) C. Rocchiccioli-Deltcheff, M. Fournier, R. Franck, and R. Thouvenot (1984). *J. Mol. Struct.* **114**, 49. (d) C. Rocchiccioli-Deltcheff, M. Fournier, R. Franck, and R. Thouvenot (1986). *Spectrosc. Lett.* **19**, 765.
66. R. A. Wheeler, M.-H. Whangbo, T. Hughbanks, R. Hoffmann, J. K. Burdett, and T. A. Albright (1986). *J. Am. Chem. Soc.* **108**, 2222.
67. M. Fournier, C. Louis, M. Che, P. Chaquin, and D. Masure (1989). *J. Catalysis* **119**, 400.
68. K. Matsumoto, A. Kobayashi, and Y. Sasaki (1975). *Bull. Chem. Soc. Japan* **48**, 1009.
69. A. Proust, R. Thouvenot, S.-G. Roh, J. K. Yoo, and P. Gouzerh (1995). *Inorg. Chem.* **34**, 4106.
70. T. R. Mohs, G. P. A. Yap, A. L. Rheingold, and E. A. Maatta (1995). *Inorg. Chem.* **34**, 9.

Printed in Belgium